

# On the three-dimensional structure of the nebula around Eta Carinae

L. Zaninetti

*Dipartimento di Fisica Generale,  
Via Pietro Giuria 1,  
10125 Torino, Italy*

---

## Abstract

The asymmetric shape of the nebula around  $\eta$ -Carinae (Homunculus) can be explained by a spherical expansion in a non-homogeneous medium. Two models are analyzed: an exponential and an inverse power law dependence for the density as a function of distance from the equatorial plane. The presence of a medium with variable density along the polar direction progressively converts the original spherical shell into a bipolar nebula. In the case of the nebula around  $\eta$ -Carinae, we know the time elapsed since the great outburst in 1840. An exact match between observed radii and velocities can be obtained by fine tuning the parameters involved, such as initial radius, initial velocity and the typical scale that characterizes the gradient in density. The observed radius and velocity of the Homunculus as a function of the polar angle in spherical coordinates can be compared with the corresponding simulated data by introducing the efficiency in a single or multiple directions. Once the 3D spatial structure of the Homunculus is obtained, we can compose the image by integrating along the line of sight. In order to simulate the observed image, we have considered a bipolar nebula with constant thickness and an optically thin emitting layer. Some simulated cuts of the relative intensity are reported and may represent a useful reference for the astronomical cuts.

*Key words:* ISM: Molecules, Stars: individual: eta- Carinae, Stars: Mass Loss, Stars: Winds, Outflows

---

## 1 Introduction

The nebula around  $\eta$ -Carinae was discovered by Thackeray (1949) and the name “the Homunculus” arises from the fact that on the photographic plates

---

*Email address:* [zaninetti@ph.unito.it](mailto:zaninetti@ph.unito.it) (L. Zaninetti ).

it resembled a small plump man, see Gaviola (1950). More details on the various aspects of  $\eta$ -Carinae can be found in Smith (2009). The structure of the Homunculus Nebula around  $\eta$ -Carinae has been analyzed with different models, we cite some of them:

- The shape and kinematics is explained by the interaction of the winds expelled by the central star at different injection velocities, see Icke (1988).
- The possibility that the nebulae around luminous blue variables (LBVs) are shaped by interacting winds has been analyzed by Nota et al. (1995). In this case a density contrast profile of the form  $\rho = \rho_0(1 + 5 \cos^4 \Theta)$  was used where  $\Theta$  is the angle to the equatorial plane.
- The origin and evolution of the bipolar nebula has been modeled by a numerical two-dimensional gasdynamic model where a stellar wind interacts with an aspherical circumstellar environment, see Frank et al. (1995).
- Cooling models form ballistic flows (that is, a pair of cones each with a spherical base) whose lateral edges become wrinkled by shear instabilities, see Dwarkadas & Balick (1998).
- The scaling relations derived from the theory of radiatively driven winds can model the outflows from luminous blue variable (LBV) stars, taking account of stellar rotation and the associated latitudinal variation of the stellar flux due to gravity darkening. In particular for a star rotating close to its critical speed, the decrease in effective gravity near the equator and the associated decrease in the equatorial wind speed results naturally in a bipolar, prolate interaction front, and therefore in an asymmetric wind, see Dwarkadas & Owocki (2002).
- Two oppositely ejected jets inflate two lobes (or bubbles) representing a unified model for the formation of bipolar lobes, see Soker (2004, 2007).
- A two-dimensional, time-dependent hydrodynamical simulation of radiative cooling, see González et al. (2004).
- Launch of material normal to the surface of the oblate rotating star with an initial kick velocity that scales approximately with the local escape speed, see Smith & Townsend (2007).
- A 3D model of wind-wind collision for X-ray emission from a supermassive star, see Parkin et al. (2009).
- Two-dimensional hydrodynamical simulations of the eruptive events of the 1840s (the great outburst) and 1890s (the minor outburst), see González et al. (2010a).

The models cited leave some questions unanswered or only partially answered:

- Which is the law of motion which regulates the expansion?
- Is it possible to model the complex three-dimensional (3D) behaviour of the velocity field of the expanding nebula?
- Is it possible to make an evaluation of the reliability of the numerical results on radius and velocity compared to observed values?

- Is it possible to evaluate the intensity of the  $H_2$  image of the nebula?
- Is it possible to build cuts of the model intensity which can be compared with existing observations?

In order to answer these questions, Section 2 describes three observed morphologies of PNs, Section 3 analyzes two different laws of motion with their associated velocities which model the aspherical expansion and Section 4 contains detailed information on how to build the image of the Homunculus as well as some sectional cuts through the relative intensity of emission.

## 2 Homunculus properties

This Section reviews the basic data of the Homunculus as well as an ad hoc formula for the latitude-dependent wind. The star  $\eta$ -Carinae had a great outburst in 1840 and at the moment of writing presents a bipolar shape called the Homunculus, its distance is 2250 pc, see Smith (2002). A more refined classification distinguishes between the large and little Homunculus, see González et al. (2006). The Homunculus has been observed at different wavelengths such as the ultraviolet and infrared by Smith et al. (2004); Smith (2009), x-ray by Corcoran et al. (2004a),  $[FeII]\lambda 16435$  by Smith (2005), ammonia by Smith et al. (2006), radio-continuum by González et al. (2006), near-infrared by Teodoro et al. (2008) and scandium and chromium lines by Bautista et al. (2009).

Referring to Table 1 in Smith (2006), we can fix the major radius at 22014 AU (0.106 pc) and the equatorial radius at 2100 AU (0.01 pc). The expansion velocity rises from  $\approx 93$  km/s at the equator to  $\approx 648$  km/s in the polar direction, see Table 1 and Figure 4 in Smith (2006). The thickness of the  $H_2$  shell is roughly 2 – 3% of the polar radius, see Smith (2006). The expansion speed of the outer  $H_2$  shell of  $\eta$ -Carinae has been fitted with the following latitude dependent velocity as given by

$$v = \frac{v_1 \left( v_2 + e^{2\lambda \cos(2\Theta)} v_1 \right)}{v_1 \left( 1 + e^{2\lambda \cos(2\Theta)} \right)}, \quad (1)$$

where the parameter  $\lambda$  controls the shape of the Homunculus,  $\Theta$  is the polar angle;  $v_1$  and  $v_2$  are the velocities in the polar and equatorial direction, see González et al. (2010a). Figure 1 reports the data of Smith (2006) as well the fit of González et al. (2010a).

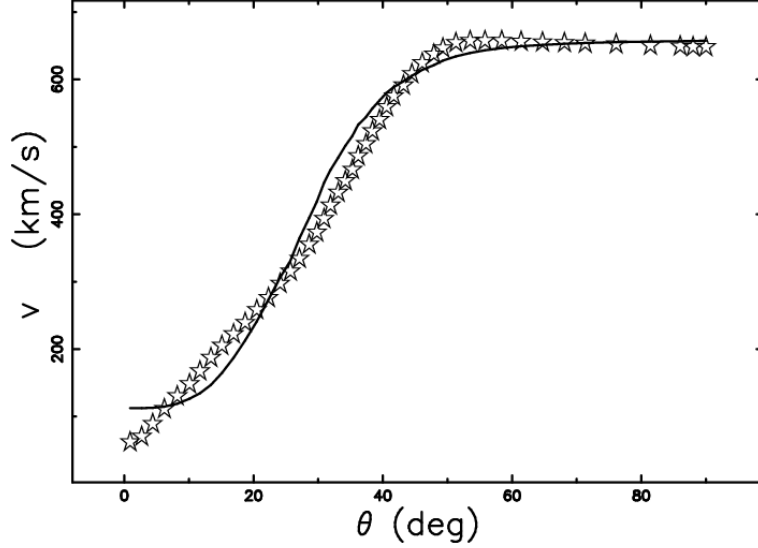


Fig. 1. Expansion velocity versus latitude of the  $H_2$  shell (Smith 2006, open stars) and fit as given by formula (1) (full line). The fitting parameters are the same as González et al. (2010a):  $\lambda=1.9$ ,  $v_1 = 670 \text{ km/s}$  and  $v_2 = 100 \text{ km/s}$ .

### 3 Law of motion

This Section presents a standard solution for the law of motion in an interstellar medium with constant density. The assumption of constant density can be generalized considering a medium which presents a decreasing behaviour in density with increasing distance from the main plane of symmetry: in particular we considered an exponential and a power law decrease in density. As a consequence two new laws of motion are deduced. In all three cases, the velocity is deduced assuming the conservation of momentum and has a simple analytical form. The resulting first order equations for the radius have separable variables and therefore the solution can be found. In the first case is possible to derive an analytical expression for the radius and in the two other cases there exists an implicit equation for the radius. A subsection deals with the simulation quality as well as along many directions.

#### 3.1 Spherical Symmetry - Conservation of Momentum

The thin layer approximation assumes that all the swept-up gas accumulates in an infinitely thin shell just behind the shock front. The conservation of radial momentum at distance  $R, P(R)$ , requires that

$$P(R) = P_0(R_0) \quad , \quad (2)$$

where  $R_0$  is the initial radius and  $P_0(R_0)$  the radial momentum at  $R_0$  evaluated when  $t = t_0$ . The conservation of the momentum gives

$$\frac{4}{3}\pi R^3 \rho \dot{R} = P_0(R_0) \quad , \quad (3)$$

where  $\dot{R}$  is the velocity of the advancing shock, see Dyson, J. E. and Williams, D. A. (1997); Padmanabhan (2001) and  $\rho$  is the density of the ambient medium. The law of motion is

$$R = R_0 \left( 1 + 4 \frac{\dot{R}_0}{R_0} (t - t_0) \right)^{\frac{1}{4}} \quad . \quad (4)$$

and the velocity

$$\dot{R} = \dot{R}_0 \left( 1 + 4 \frac{\dot{R}_0}{R_0} (t - t_0) \right)^{-\frac{3}{4}} \quad . \quad (5)$$

We can derive  $\dot{R}_0$  from equation (4) and insert it in equation (5)

$$\dot{R} = \frac{1}{4(t - t_0)} \frac{R^4 - R_0^4}{R_0^3} \left( 1 + \frac{R^4 - R_0^4}{R_0^4} \right)^{-\frac{3}{4}} \quad . \quad (6)$$

The astrophysical units are:  $t_4$  and  $t_{0,4}$  which are  $t$  and  $t_0$  expressed in  $10^4$  yr units,  $R_{pc}$  and  $R_{0,pc}$  which are  $R$  and  $R_0$  expressed in pc,  $\dot{R}_{kms}$  and  $\dot{R}_{0,kms}$  which are  $\dot{R}$  and  $\dot{R}_0$  expressed in  $km/s$ . Therefore the previous formula becomes

$$\dot{R}_{kms} = 24.49 \frac{1}{(t_4 - t_{0,4})} \frac{R_{pc}^4 - R_{0,pc}^4}{R_{0,pc}^3} \left( 1 + \frac{R_{pc}^4 - R_{0,pc}^4}{R_{0,pc}^4} \right)^{-\frac{3}{4}} \quad . \quad (7)$$

An interesting quantity can be the swept mass at a distance  $R$  from the origin

$$M = \frac{4}{3}\pi R^3 \rho \quad . \quad (8)$$

The density can be

$$\rho = 1.4 n_1 m_H \frac{g}{cm^3} = 1.4 \times 1.6610^{-24} n_1 \frac{g}{cm^3} \quad , \quad (9)$$

where  $n_1$  is the number density expressed in units of particle  $cm^{-3}$  and the factor 1.4 takes into account elements heavier than hydrogen. Introducing the

solar mass,  $M_\odot$ , the swept-up mass is

$$M = 0.143 R_1^3 n_1 M_\odot \quad , \quad (10)$$

where  $R_1$  is the radius expressed in pc units.

### 3.2 Exponentially varying medium

The number density of an exponentially varying medium is described by

$$n(z) = n_0 \exp\left(-\frac{z}{h}\right) \quad , \quad (11)$$

where  $z$  is the distance from the equatorial plane,  $n_0$  is the number of particles at  $R = R_0$  and  $h$  is the scale height.

A three-dimensional (3D) expansion will be characterized by the following properties

- Dependence from the instantaneous radius of the shell on the latitude angle  $\theta$  which has a range  $[-90^\circ \leftrightarrow +90^\circ]$ .
- Independence of the instantaneous radius of the shell from  $\phi$ , the azimuthal angle in the x-y plane, which has a range  $[0^\circ \leftrightarrow 360^\circ]$ .

The mass,  $M$ , swept-up along a solid angle  $\Delta \Omega$ , between 0 and  $R$  is

$$M(R) = \frac{\Delta \Omega}{3} 1.4 m_H n_0 I_m(R) + \frac{4}{3} \pi R_0^3 n_0 m_H 1.4 \quad , \quad (12)$$

where  $m_H$  is the mass of hydrogen and

$$I_m(R) = \int_{R_0}^R r^2 \exp\left(-\frac{r \sin(\theta)}{h}\right) dr \quad , \quad (13)$$

where  $R_0$  is the initial radius. The integral is

$$I_m(R) = \frac{h \left( 2 h^2 + 2 R_0 h \sin(\theta) + R_0^2 (\sin(\theta))^2 \right) e^{-\frac{R_0 \sin(\theta)}{h}}}{(\sin(\theta))^3} - \frac{h \left( 2 h^2 + 2 R h \sin(\theta) + R^2 (\sin(\theta))^2 \right) e^{-\frac{R \sin(\theta)}{h}}}{(\sin(\theta))^3} \quad . \quad (14)$$

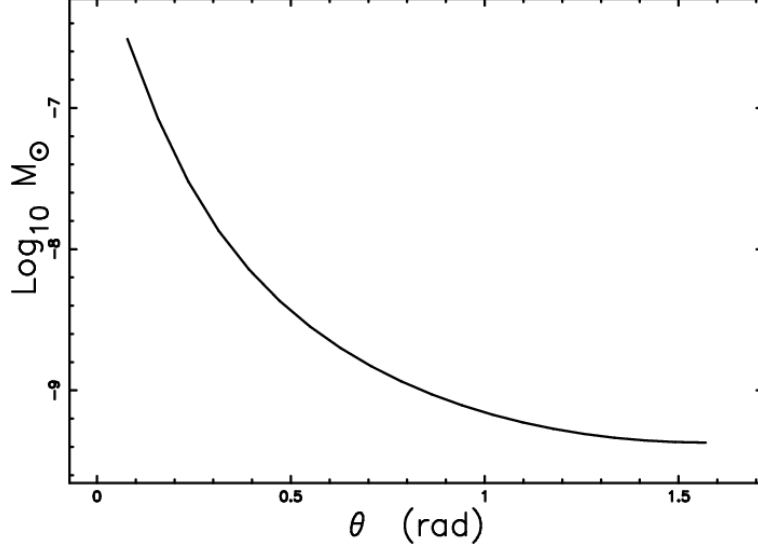


Fig. 2. Decimal logarithm of swept-up mass when  $R = 0.05 pc$ ,  $n_1 = 1$  and  $\Delta \Omega = 1$ . Physical parameters as in Table 1.

In this case, the swept mass is a function of the latitude angle  $\theta$  and can be plotted assuming  $\Delta \Omega = 1$ , see Figure 2.

This numerical evaluation gives a simple explanation for the asymmetry of the nebula around  $\eta$ -Carinae: a smaller mass being swept means a greater velocity of the advancing radius of the nebula.

Conservation of momentum gives

$$M(R)\dot{R} = M(R_0)\dot{R}_0 \quad . \quad (15)$$

In this differential equation of the first order in  $R$ , the variables can be separated and an integration term-by-term gives

$$\int_{R_0}^R M(r)dr = M(R_0)\dot{R}_0 \times (t - t_0) \quad , \quad (16)$$

where  $t$  is the time and  $t_0$  is the time at  $R_0$ . The resulting non-linear equation  $\mathcal{F}_{NL}$ , is equation (17) in Zaninetti (2009). The radius  $R_{pc}$  as function of the time, is found by a numerical method, in the case of  $\eta$ -Carinae the age is 158 *yr* and therefore  $t_4 - t_{0,4} = t_0/(10^4 yr) = 0.0158$ .

### 3.3 Power law medium

A possible form for a power law profile of the medium surrounding the Homunculus nebula is

$$n(z) = n_0 \left( \frac{z}{R_0} \right)^{-\alpha} , \quad (17)$$

where  $z = R \times \sin(\theta)$  is the distance from the equatorial plane,  $R$  is the instantaneous radius of expansion,  $n_0$  is the number of particles at  $R = R_0$  and  $\alpha$  is a coefficient  $> 0$ .

The swept-up mass,  $M$ , along a solid angle  $\Delta \Omega$  between 0 and  $R$  is

$$M(R) = \frac{\Delta \Omega}{3} 1.4 m_H n_0 I_m(R) + \frac{4}{3} \pi R_0^3 n_0 m_H 1.4 , \quad (18)$$

where

$$I_m(R) = \int_{R_0}^R r^2 \left( \frac{r \sin(\theta)}{R_0} \right)^{-\alpha} dr , \quad (19)$$

where  $R_0$  is the initial radius. Integrating gives:

$$I_m(R) = \frac{R^3 \left( \frac{R \sin(\theta)}{R_0} \right)^{-\alpha}}{3 - \alpha} . \quad (20)$$

The resulting non-linear equation  $\mathcal{F}_{NL}$  of motion expressed in astrophysical units can be obtained by eqns. (15) and (16) and is

$$\begin{aligned} \mathcal{F}_{NL} = & -R_{0,pc}^4 \alpha^2 + R_{pc} R_{0,pc}^3 \alpha^2 + R_{pc} R_{0,pc}^3 (\sin(\theta))^{-\alpha} \alpha \\ & + 7.0 R_{0,pc}^4 \alpha - R_{0,pc}^4 (\sin(\theta))^{-\alpha} \alpha - 7.0 R_{pc} R_{0,pc}^3 \alpha \\ & + 3 R_{0,pc}^4 (\sin(\theta))^{-\alpha} - 12 R_{0,pc}^4 - 4.0 R_{pc} R_{0,pc}^3 (\sin(\theta))^{-\alpha} \\ & + R_{pc}^{-\alpha+4.0} R_{0,pc}^\alpha (\sin(\theta))^{-\alpha} + 12 R_{pc} R_{0,pc}^3 \\ & - 0.122 R_{0,pc}^3 \dot{R}_{0,kms} (t_4 - t_{0,4}) \\ & - 0.01 R_{0,pc}^3 \dot{R}_{0,kms} (t_4 - t_{0,4}) \alpha^2 \\ & + 0.0714 R_{0,pc}^3 \dot{R}_{0,kms} (t_4 - t_{0,4}) \alpha = 0 , \end{aligned} \quad (21)$$

where  $t_4$  and  $t_{0,4}$  are  $t$  and  $t_0$  expressed in  $10^4$  yr units,  $R_{pc}$  and  $R_{0,pc}$  are  $R$  and  $R_0$  expressed in pc,  $\dot{R}_{kms}$  and  $\dot{R}_{0,kms}$  are  $\dot{R}$  and  $\dot{R}_0$  expressed in  $km/s$  and  $\theta$  is expressed in radians.



It is not possible to find  $R_{pc}$  analytically and a numerical method must be implemented. In our case, in order to find the root of  $\mathcal{F}_{NL}$ , the FORTRAN SUBROUTINE ZRDDR from Press et al. (1992) has been used. The unknown parameters,  $R_{0,pc}$  and  $\dot{R}_{0,kms}$ , are found from different runs of the code,  $t_4 - t_{0,4}$  is an input parameter.

### 3.4 Quality of the simulations

As in Zaninetti (2009), two parameters are introduced to assess the quality of the simulations. The first,  $\epsilon$ , compares observed and simulated quantities:

$$\epsilon = \left(1 - \frac{|(R_{pc,obs} - R_{pc,num})|}{R_{pc,obs}}\right) \cdot 100, \quad (22)$$

where  $R_{pc,obs}$  is observed radius, in parsec and  $R_{pc,num}$  is the radius from our simulation in parsec.

The second defines an observational reliability,  $\epsilon_{obs}$ , over the whole range of the latitude angle  $\theta$ ,

$$\epsilon_{obs} = 100 \left(1 - \frac{\sum_j |R_{pc,obs} - R_{pc,num}|_j}{\sum_j R_{pc,obs,j}}\right), \quad (23)$$

where the index  $j$  varies from 1 to the number of available observations. Those of the Homunculus are represented by Table 1 in Smith (2006).

### 3.5 Simulations quality for exponentially varying medium

A typical set of parameters which allows the Homunculus nebula around  $\eta$ -Carinae to be simulated in the presence of a medium whose density decreases exponentially is reported in Table 1. Table 2 presents numbers concerning the quality of fit.

The bipolar character of the Homunculus is shown in Figure 3. In order to better visualize the two lobes, Figure 4 and Figure 5 show the radius and velocity as a function of the angular position  $\theta$ . The orientation of the observer is characterized by the three Euler angles ( $\Phi, \Theta, \Psi$ ), see Goldstein et al. (2002); different Euler angles produce different observed shapes.

The velocity field is shown in Figure 6.

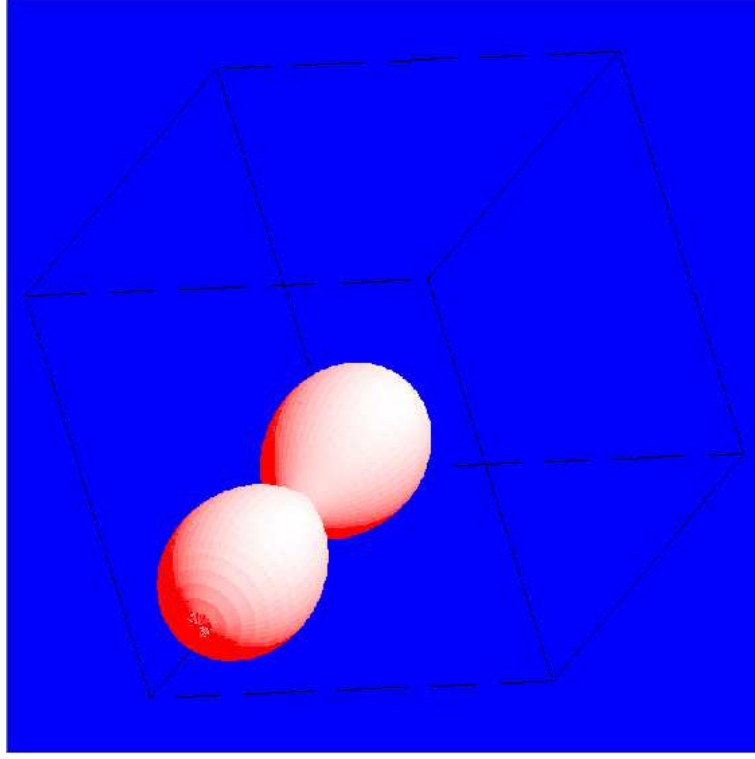


Fig. 3. Simulations lead to this picture of the Homunculus for an exponentially varying medium. The orientation of the figure is characterized by the Euler angles , which are  $\Phi=130^\circ$ ,  $\Theta=40^\circ$  and  $\Psi=-140^\circ$ . Physical parameters as in Table 1.

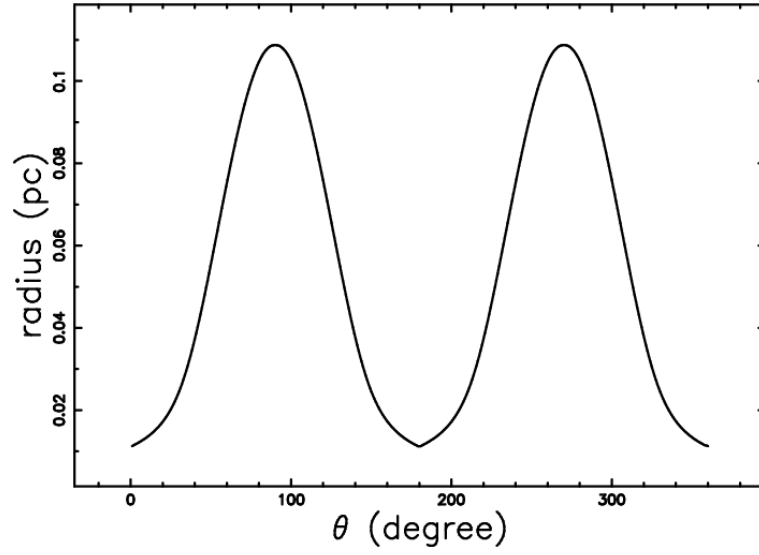


Fig. 4. Radius as a function of latitude for an exponentially varying medium (dotted line) and astronomical data with error bar. Physical parameters as in Table 1.

Table 1

Parameter values used to simulate the observations of the Homunculus nebula for a medium varying exponentially (first 4 values) or a power law (2nd set of 4 values)

Initial expansion velocity, $\dot{R}_{0,1}$ [km s <sup>-1</sup> ]	8000
Age ( $t_4 - t_{0,4}$ ) [10 <sup>4</sup> yr]	0.0158
Scaling h [pc]	0.0018
Initial radius $R_0$ [pc]	0.001
Initial expansion velocity, $\dot{R}_{0,1}$ [km s <sup>-1</sup> ]	40,000
Age ( $t_4 - t_{0,4}$ ) [10 <sup>4</sup> yr]	0.0158
Initial radius $R_0$ [pc]	0.0002
Power law coefficient $\alpha$	2.4

Table 2

Agreement between observations and simulations for the Homunculus nebula, for an exponentially varying medium.

	<i>radius velocity</i>	
$\epsilon(\%) - \text{polar direction}$	97	99
$\epsilon(\%) - \text{equatorial direction}$	87	19
$\epsilon_{obs}(\%)$	85	75

The accuracy with which our code reproduces the spatial shape and the velocity field over 18 directions of the Homunculus nebula as given by formula (23) is reported in Table 2. From a careful analysis of Table 2 we can conclude that the spatial shape over 18 directions is well modeled by an exponential medium,  $\epsilon_{obs} = 85\%$ . The overall efficiency of the field is smaller  $\epsilon_{obs} = 75\%$ . We can therefore conclude that formula (23) which gives the efficiency over all the range of polar angles represents a better way to describe the results in respect to the efficiency in a single direction as given by formula (22).

### 3.6 Simulations quality for power law medium

For assumed parameters see Table 1, Table 3 reports the accuracy of radius and velocity in two directions.

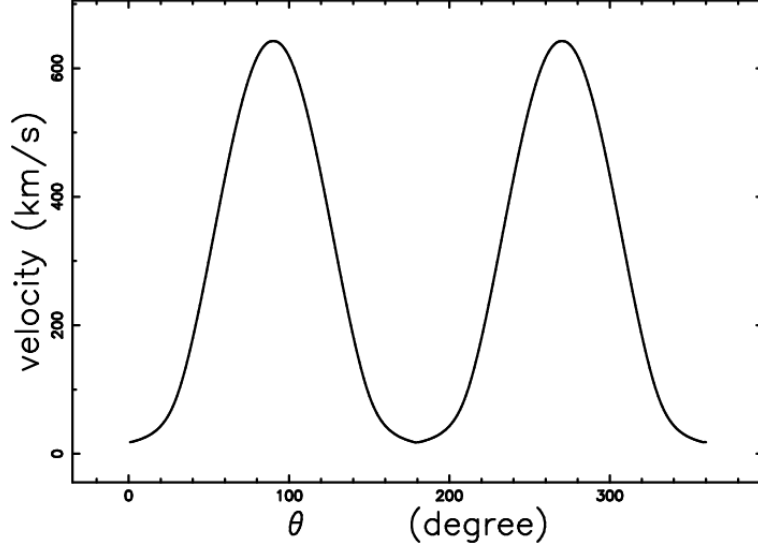


Fig. 5. Velocity as a function of latitude for an exponentially varying medium (dotted line) and astronomical data with error bar Physical parameters as in Table 1.

Table 3

Agreement between model for a power law medium and observations.

	<i>radius velocity</i>	
$\epsilon(\%) - \text{polar direction}$	78	76
$\epsilon(\%) - \text{equatorial direction}$	6	2
$\epsilon_{obs}(\%)$	79	73

## 4 Image

An image of an astrophysical object is composed in a simulation by combining the intensities that characterize different points. For an optically thin medium the transfer equation provides the emissivity to be multiplied with the distance in the line of sight. The transfer equation has been analyzed in Section 5.1 of Zaninetti (2009). The Homunculus nebula was observed through emission-line spectra such as  $H_2$  and  $[FeII]$ , see Smith (2006). We now outline a possible source of radiation. The volume emission coefficient of the transition  $j_{21}$  is

$$j_{21} = \frac{n_2 A_{21} h \nu_{21}}{4\pi} \quad , \quad (24)$$

where level 1 is the lower level, level 2 is the upper level,  $n_2$  is the gas number density,  $n_2 A_{21}$  is the rate of emission of photons from a unit volume,  $A_{21}$  is

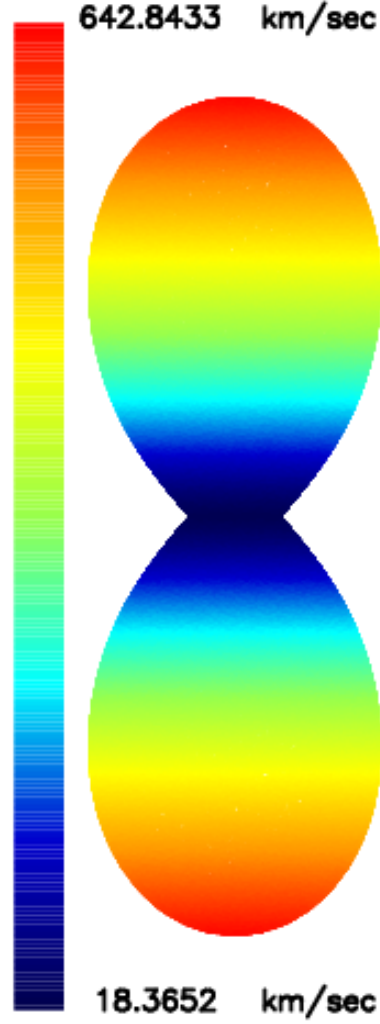


Fig. 6. Map of the expansion velocity for an exponentially varying medium. Physical parameters as in Table 1.

the Einstein coefficient for the transition,  $h$  is the Planck constant and  $\nu_{21}$  is the frequency under consideration, see Hartigan (2008). In the case of an optically thin medium, the intensity of the emission  $I_{21}$  is the integral along the line of sight

$$I_{21} = \int j_{21} dl \quad . \quad (25)$$

In the case of a constant gas number density

$$I_{21} \propto l \quad , \quad (26)$$

where  $l$  is the appropriate length, which in astrophysical diffuse objects depends on the orientation of the observer.

The numerical algorithm which allows us to build the image is now outlined.

- An empty (value=0) memory grid  $\mathcal{M}(i, j, k)$  which contains  $NDIM^3$  pixels is considered
- We first generate an internal 3D surface by rotating the ideal image  $180^\circ$  around the polar direction and a second external surface at a fixed distance  $\Delta R$  from the first surface. As an example, we fixed  $\Delta R = 0.03R_{max}$ , where  $R_{max}$  is the maximum radius of expansion, see Smith et al. (2006). The points on the memory grid which lie between the internal and external surfaces are memorized on  $\mathcal{M}(i, j, k)$  (value=1).
- Each point of  $\mathcal{M}(i, j, k)$  has spatial coordinates  $x, y, z$  which can be represented by the following  $1 \times 3$  matrix,  $A$ ,

$$A = \begin{bmatrix} x \\ y \\ z \end{bmatrix} . \quad (27)$$

The orientation of the object is characterized by the Euler angles  $(\Phi, \Theta, \Psi)$  and therefore by a total  $3 \times 3$  rotation matrix,  $E$ , see Goldstein et al. (2002). The matrix point is represented by the following  $1 \times 3$  matrix,  $B$ ,

$$B = E \cdot A \quad . \quad (28)$$

- The intensity map is obtained by summing the points of the rotated images along a particular direction.

An ideal image of the Homunculus nebula having the polar axis aligned with the z-direction which means polar axis along the z-direction, is shown in Figure 7 and this should be compared with the  $H_2$  emission structure reported in Figure 4 of Smith (2006). A model for a realistically rotated Homunculus is shown in Figure 8. This should be compared with Figure 1 in Smith & Gehrz (2000) or Figure 1 in Smith (2006).

The rotated image exhibits a double ring and an intensity enhancement in the central region which characterizes the little Homunculus, see Smith (2002); Ishibashi et al. (2003); Smith (2005); González et al. (2006). Figure 9 and Figure 10 show two cuts through the Homunculus nebula without and with rotation. The intensity enhancement is due to a projection effect and is an alternative for the theory that associates the little Homunculus with an eruption occurring some time after the Great Eruption, see Ishibashi et al. (2003); Smith (2005). We briefly recall that a central enhancement is visible in one of the various morphologies characterizing planetary nebulae. This can be compared with the model  $BL_1 - F$  in Figure 3 of the Atlas of synthetic line profiles by Morisset & Stasinska (2008).

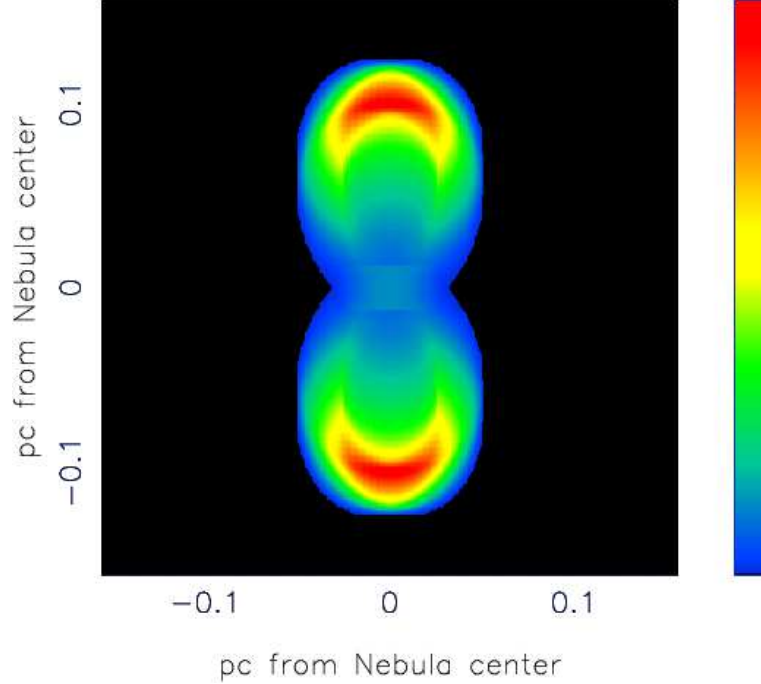


Fig. 7. Map of the theoretical intensity of the Homunculus nebula in the presence of an exponentially varying medium. Physical parameters as in Table 1. The three Euler angles characterizing the orientation are  $\Phi=180^\circ$ ,  $\Theta=90^\circ$  and  $\Psi=0^\circ$ . This combination of Euler angles corresponds to the rotated image with the polar axis along the z-axis.

Such cuts are common when analyzing planetary nebulae. As an example Figure 4 in Jacoby et al. (2001) reports a nearly symmetrical profile of the intensity in the [OIII] image of A39, a nearly spherical planetary nebula. Another example is the east-west cut in  $H\beta$  for the elliptical Ring nebula, crossing the center of the nebula, see Figure 1 in Garnett & Dinerstein (2001). Such intensity cuts are not yet available for  $\eta$ -Carinae and therefore can represent a new target for the observers.

## 5 Conclusions

**Law of motion** We have analyzed the law of motion determined by the conservation of radial momentum under two circumstances: exponential or power law variation of the density of the interstellar medium. The two non-linear equations of motion are given by formulae (17) in Zaninetti (2009) and 21). A comparison of the observed and simulated profiles (Tables 2 and 3), shows that the profiles are better described by an exponential variation than by a power law. Here we have assumed that all the swept-up mass resides in a thin shell beyond the advancing surface. In the case of clumpy material this approximation can be refined by introducing the porosity  $p$ . Then, the

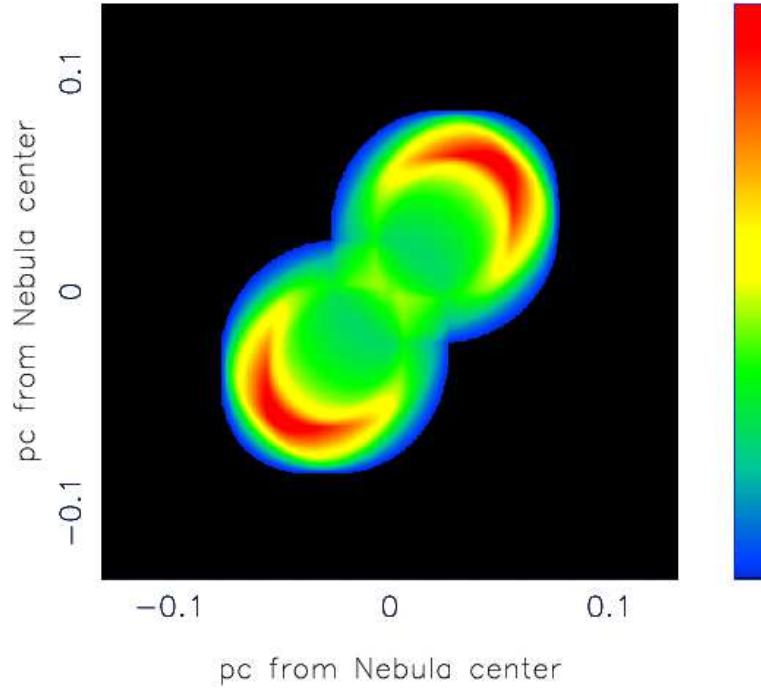


Fig. 8. Model map of the Homunculus nebula rotated in accordance with the observations, for an exponentially varying medium. Physical parameters as in Table 1. The three Euler angles characterizing the orientation of the observer are  $\Phi=130^\circ$ ,  $\Theta=40^\circ$  and  $\Psi=-140^\circ$ . This combination of Euler angles corresponds to the observed image.

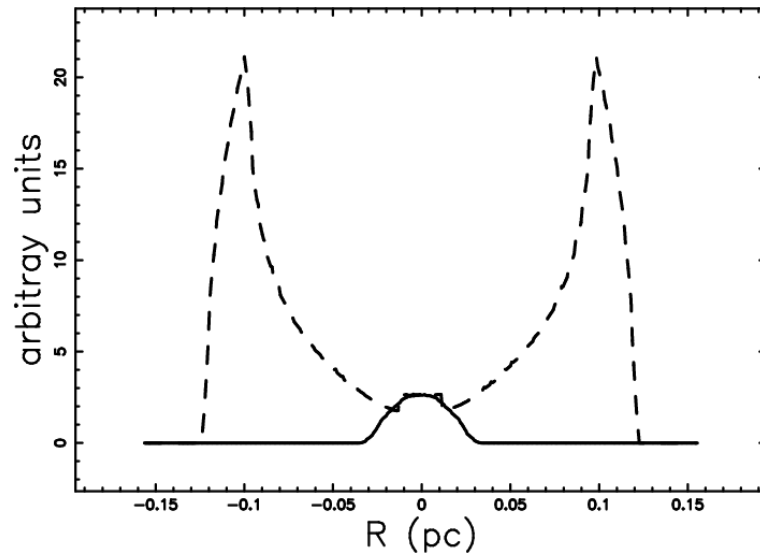


Fig. 9. Two cuts of the model intensity across the center of the Homunculus nebula for an exponentially varying medium: equatorial cut (full line) and polar cut (dotted line). Parameters as in Figure 7.



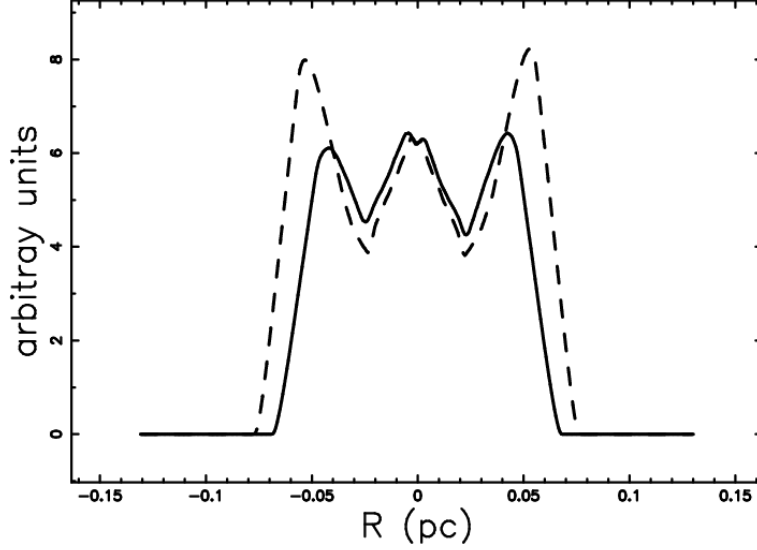


Fig. 10. Two cuts of the model intensity across the center of the realistically rotated Homunculus nebula for an exponentially varying medium: equatorial cut (full line) and polar cut (dotted line). Parameters as in Figure 8.

accumulated mass is  $M^{1/p}$  rather than  $M$ .

We briefly recall that the general principles of mass addition to astrophysical flows via hydrodynamic mixing have been investigated by Hartquist et al. (1986) and Pittard (2007). In order to fix the porosity parameter  $p$  the equation of motion along the polar direction should be provided in the form

$$R(t) = r_{obs} t^{\alpha_{obs}} \quad , \quad (29)$$

where the two parameters  $r_{obs}$  and  $\alpha_{obs}$  are found from an analysis of the observational data. As an example the data over a 10 year period of SN 1993J can be approximated by a power law dependence of the type  $R \propto t^{0.82}$ , see Marcaide et al. (2009).

**Images** Assuming an optically thin medium, it is possible to make a model image of the Homunculus nebula once two hypotheses are made:

- (1) The thickness of the emitting layer,  $\Delta R$ , is the same everywhere  $\Delta R = 0.03 R_{max}$ , where  $R_{max}$  is the maximum radius of expansion.
- (2) The density of the emitting layer is constant everywhere

A 2D image of the Homunculus nebula is shown in Figure 7 and a non-rotated image in Figure 8. Our model provides an explanation for the emission maps in e.g. X-rays (0.2 -1.5 keV) by CHANDRA. An inspection of Figure 1 in Corcoran et al. (2004a) shows that the next generation of X-ray observatories may resolve the double ring as observed in the near infrared, see Figure 4 of Smith (2006) and our simulation in Figure 8. The validity of our assumptions

can be checked by looking at cuts in intensity over the various bands. We recall that cuts in intensity allow to fix the thickness of the swept-up layer of a planetary nebula such as A39 where  $\frac{\Delta R}{R} \approx \frac{10'}{77'}$ , see Jacoby et al. (2001).

## References

- Bautista, M. A., Ballance, C., Gull, T. R., et al. Scandium and chromium in the strontium filament in the Homunculus of  $\eta$ Carinae. *Mon. Notices R. astr. Soc.* 393 , 1503-1512, 2009.
- Corcoran, M. F., Hamaguchi, K., Gull, T., & Davidson, K. Waiting in the Wings: Reflected X-Ray Emission from the Homunculus Nebula. *Astrophys. J.* 613, 381-386, 2004.
- Dwarkadas, V. V. & Balick, B. On the Formation of the Homunculus Nebula around eta Carinae. *Astronom. J.* 116 ,829-839, 1998.
- Dwarkadas, V. V. & Owocki, S. P. Radiatively Driven Winds and the Shaping of Bipolar Luminous Blue Variable Nebulae. *Astrophys. J.* 581, 1337-1343, 2002.
- Dyson, J. E. and Williams, D. A., The physics of the interstellar medium, Institute of Physics Publishing , Bristol , 1997.
- Frank, A., Balick, B., & Davidson, K. The homunculus of Eta Carinae: an interacting stellar winds paradigm. *Astrophys. J. L.* 441 , L77-L80, 1995.
- Garnett, D. R. & Dinerstein, H. L. Spatially Resolved O II Recombination Line Observations of the Ring Nebula, NGC 6720. *Astrophys. J.* 558 ,145-156, 2001.
- Gaviola, E., Eta Carinae. I. The Nebulosity. *Astrophys. J.* 111 ,408-415, 1950.
- Goldstein, H., Poole, C., & Safko, J. Classical mechanics, Addison-Wesley , San Francisco , 2002.
- González, R. F., de Gouveia Dal Pino, E. M., Raga, A. C., & Velazquez, P. F. Gasdynamical Simulations of the Large and Little Homunculus Nebulae of  $\eta$  Carinae, *Astrophys. J. L.* 600 , L59-L62, 2004.
- González, R. F., Montes, G., Cantó, J., & Loinard, L. Predicted radio-continuum emission from the little Homunculus of the eta Carinae nebula, *Mon. Notices R. astr. Soc.* 373, 391-396, 2006.
- González, R. F., Villa, A. M., Gómez, G. C., et al., Revisiting 2D numerical models for the 19th century outbursts of  $\eta$  Carinae, *Mon. Notices R. astr. Soc.* 402, 1141-1148, 2010.
- Hartigan, P. Measurement of Physical Conditions in Stellar Jets in: Bacciotti, F. (Ed.) , *Lecture Notes in Physics*, Springer Verlag, Berlin, pp 15-25,2008.
- Hartquist, T. W., Dyson, J. E., Pettini, M., & Smith, L. J. Mass-loaded astronomical flows. I - General principles and their application to RCW 58. *Mon. Notices R. astr. Soc.* 221 ,715-726, 1986.
- Icke, V. Blowing bubbles, *Astron. Astrophys.* 202, 177-188, 1988.
- Ishibashi, K., Gull, T. R., Davidson, K., Smith, N., & Lanz, T. Discovery of

- a Little Homunculus within the Homunculus Nebula of eta Carinae, *Astronom. J.* 125, 3222-3236, 2003.
- Jacoby, G. H., Ferland, G. J., & Korista, K. T. The Planetary Nebula A39: An Observational Benchmark for Numerical Modeling of Photoionized Plasmas. *Astrophys. J.* 560, 272-286, 2001.
- Marcaide, J. M., Martí-Vidal, I., Alberdi, A., & Pérez-Torres, M. A. A decade of SN 1993J: discovery of radio wavelength effects in the expansion rate. *Astron. Astrophys.* 505, 927-945, 2009
- Morisset, C. & Stasinska, G. An atlas of synthetic line profiles of Planetary Nebulae, *Revista Mexicana de Astronomia y Astrofisica* 44, 171-180, 2008.
- Nota, A., Livio, M., Clampin, M., & Schulte-Ladbeck, R., Nebulae around Luminous Blue Variables: A Unified Picture. *Astrophys. J.* 448, 788-789, 1995.
- Padmanabhan, P. Theoretical astrophysics. Vol. II: Stars and Stellar Systems, Cambridge University Press, Cambridge, MA, 2001.
- Parkin, E. R., Pittard, J. M., Corcoran, M. F., Hamaguchi, K., & Stevens, I. R. 3D modelling of the colliding winds in  $\eta$  Carinae - evidence for radiative inhibition, *Mon. Notices R. astr. Soc.* 394, 1758-1774, 2009.
- Pittard, J. M. Mass-Loaded Flows, in: Hartquist, T. W., Pittard, J. M., & Falle, S. A. E. G. (Eds.), *Diffuse Matter from Star Forming Regions to Active Galaxies*, Springer, Dordrecht, pp 245-255, 2007.
- Press, W. H., Teukolsky, S. A., Vetterling, W. T., & Flannery, B. P., *Numerical recipes in FORTRAN. The art of scientific computing*, Cambridge University Press, Cambridge, 1992.
- Smith, N. Dissecting the Homunculus nebula around Eta Carinae with spatially resolved near-infrared spectroscopy. *Mon. Notices R. astr. Soc.* 337, 1252-1268, 2002.
- Smith, N. Doppler tomography of the Little Homunculus: high-resolution spectra of FeII lambda 16435 around Eta Carinae. *Mon. Notices R. astr. Soc.* 357, 1330-1336, 2005.
- Smith, N. The Structure of the Homunculus. I. Shape and Latitude Dependence from H2 and Fe II Velocity Maps of eta Carinae. *Astrophys. J.* 644, 1151-1163, 2006
- Smith, N., All Things Homunculus, arXiv:0906.2204, 2009.
- Smith, N., Brooks, K. J., Koribalski, B. S., & Bally, J. Cleaning Up  $\eta$  Carinae: Detection of Ammonia in the Homunculus Nebula. *Astrophys. J. L.* 645, L41-L44, 2006.
- Smith, N. & Gehrz, R. D. Recent Changes in the Near-Infrared Structure of  $\eta$  Carinae. *Astrophys. J. L.* 529, L99-L102, 2000.
- Smith, N., Morse, J. A., Gull, T. R., et al. Kinematics and Ultraviolet to Infrared Morphology of the Inner Homunculus of  $\eta$  Carinae. *Astrophys. J.* 605, 405-424, 2004.
- Smith, N. & Townsend, R. H. D. The Structure of the Homunculus. III. Forming a Disk and Bipolar Lobes in a Rotating Surface Explosion. *Astrophys. J.* 666, 967-975, 2007.

- Soker, N. Why a Single-Star Model Cannot Explain the Bipolar Nebula of  $\eta$  Carinae. *Astrophys. J.* 612 , 1060-1064, 2004.
- Soker, N. Comparing  $\eta$  Carinae with the Red Rectangle, *Astrophys. J.* 661, 490-495, 2007.
- Teodoro, M., Damineli, A., Sharp, R. G., Groh, J. H., & Barbosa, C. L. Near-infrared integral field spectroscopy of the Homunculus nebula around  $\eta$  Carinae using Gemini/CIRPASS. *Mon. Notices R. astr. Soc.* 387 , 564-576, 2008.
- Thackeray, A. D. Nebulosity surrounding eta Carinae, *The Observatory* 69, 31-33, 1949.
- Zaninetti, L. Scaling for the intensity of radiation in spherical and aspherical planetary nebulae, *Mon. Notices R. astr. Soc.* 395, 667-691, 2009.